ANALYSIS OF SEISMIC WAVES CROSSING THE SANTA CLARA BASIN USING THE THREE-COMPONENT MUSIQUE ARRAY ALGORITHM

Manuel Hobiger[1,*], Cécile Cornou[1], Pierre-Yves Bard[1], Nicolas Le Bihan[2]
[1] ISTerre, CNRS, IRD, IFSTTAR, Université de Savoie, Université Joseph Fourier, Grenoble, France
[*] now at: Federal Institute for Geosciences and Natural Resources (BGR), Hannover, Germany, manuel.hobiger@bgr.de
[2] GIPSA-Lab, CNRS, Grenoble, France

ABSTRACT

The MUSIQUE algorithm (Hobiger *et al.*, 2011) was designed to analyze seismic signals recorded by arrays of three-component seismic sensors. The algorithm is based on the MUSIC algorithm (Schmidt, 1986) and the quaternion-MUSIC algorithm (Miron *et al.*, 2005). The first step is the application of the MUSIC algorithm in order to estimate azimuth and velocity of incident waves and discriminate between Love and possible Rayleigh waves. In a second step, the polarization parameters of Rayleigh waves are analyzed using quaternion-MUSIC: the retrograde or prograde sense of Rayleigh wave particle motion and the ellipticity are determined. We applied the MUSIQUE algorithm to seismic wave field recordings by the San Jose Dense Seismic Array. This array has been installed in 1999 in the Evergreen Basin, a sedimentary basin in the Eastern Santa Clara Valley. The data recordings for 22 different regional earthquakes, located between 40 and 600 km from the array and covering all possible azimuths, have been analyzed. We estimate the azimuthal distribution and the energy partition of the different surface wave types that contributed about 40% to the total signal energy. Large amounts of scattered Love waves are systematically coming from the south. For close events to the north, the first higher mode of Love waves dominates the wave field. Scattered retrograde and prograde Rayleigh waves are mainly coming from the eastern border or from the southern and eastern borders, respectively. Dispersion and ellipticity curves obtained by combining results of the different events indicate a shear-wave velocity profile faster than the one given by the Bay area model.

INTRODUCTION

Based on the MUSIC (Schmidt, 1986) and quaternion-MUSIC (Miron *et al.*, 2005, 2006) algorithms, the MUSIQUE algorithm (Hobiger *et al.*, 2011) is an advanced three-component seismic array processing technique. In addition to the estimation of azimuth and slowness (*i.e.* the wave vector) of incoming waves, the algorithm allows the identification of Love and Rayleigh waves and the estimation of the associated polarization parameters (ellipticity and sense of rotation of the Rayleigh wave particle motion as a function of frequency). The distinction between prograde and retrograde particle motion may be helpful to separate the fundamental and higher Rayleigh wave modes or to better identify the left and right flanks of the fundamental Rayleigh wave ellipticity peak.

In this paper, the MUSIQUE technique is applied to earthquake data recorded between 1999 and 2004 by the San Jose Dense Seismic Array in California, a temporary seismological array. The array was located near the eastern edge of the Santa Clara Valley, where deep sedimentary layers form the Evergreen Basin. The south-western edge of the Santa Clara Valley is formed by the Cupertino basin, which is separated from the Evergreen Basin by a subsurface ridge. The geology of the Evergreen Basin is shown in Fig. 1.

A previous study using data of the San Jose Dense Seismic Array was published by Frankel *et al.* (2001). They found that the amplification of seismic waves is stronger towards the south-western edge of the Evergreen Basin. Furthermore, they observed patterns of waves traveling across the array. For earthquakes located east of the basin, surface waves from the south follow the direct S-wave arrivals. Frankel *et al.* (2001) identified these surface waves as Love waves which are probably generated by S-wave scattering at the southern border of the Santa Clara Valley.

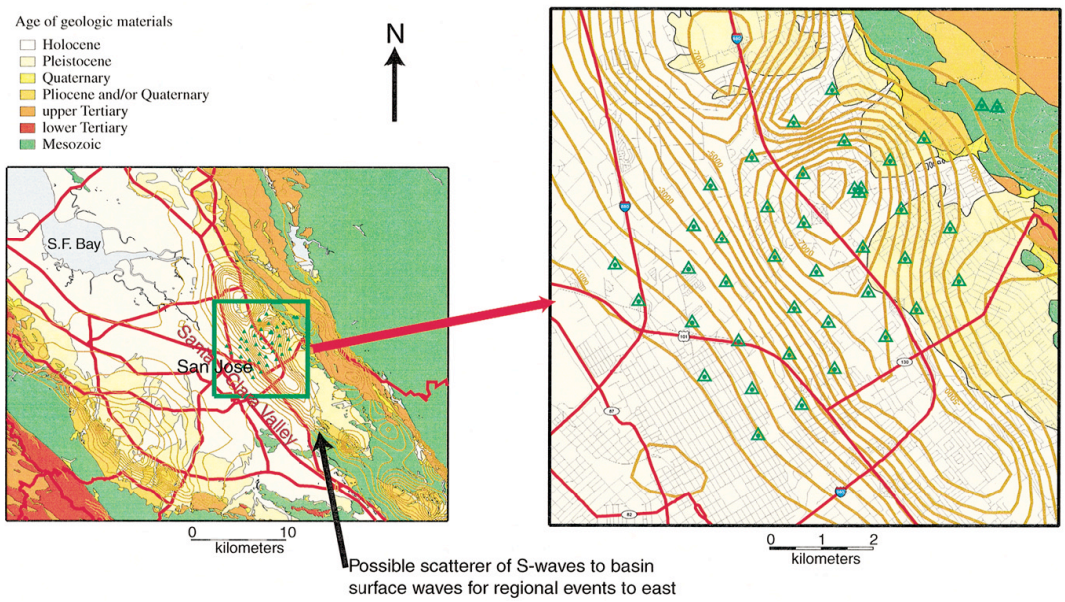

Fig. 1. (Left) Map showing the superficial geology (by Wentworth, 1997) of the Santa Clara Valley and the location of the San Jose Dense Seismic Array. In the zoom on the array (right), the array stations and the depth contour layers (by Brocher et al., 1997) of the Evergreen Basin are shown in 500-m-intervals. The basin reaches a maximum depth of about 8 km. [Figure extracted from Frankel et al., 2001]

Another study using the San Jose Dense Seismic Array was performed by Hartzell *et al.* (2003), who investigated the site response for local and regional earthquakes and identified surface waves generated or scattered at the edges of the Santa Clara Valley and near the western edge of the Evergreen Basin. Hartzell *et al.* (2006) developed a detailed 3D velocity model of the Santa Clara Valley and showed the importance of surface waves crossing the basin by ground motion modeling.

In a further study by Hartzell *et al.* (2010), it was shown that the maximum of amplification occurs at the southern edge of the basin for the horizontal motion, whereas it occurs at the deepest parts of the basin for the vertical component. The authors suggest that this can be attributed to differences in the interaction with the basin shape for Love and Rayleigh waves or that Love waves are more influenced by the lower shear wave velocity region at the south-western edge of the basin.

Fletcher *et al.* (2003) analyzed the data of a different array covering the whole Santa Clara Valley. They investigated the P- and S-wave arrival times from both local deep events and teleseismic events and found that the arrivals are delayed for stations located in the Evergreen or Cupertino Basins, but arrive earlier for stations located on the ridge between both basins. Furthermore, they determined that the attenuation is larger in the basins than on the ridge. Dolenc *et al.* (2005a) used the same array recordings and showed that the P-wave arrival time delays and amplification parameters for teleseismic events are correlated. Another study by Dolenc *et al.* (2005b), which was based on the same array, analyzed microtremor records. This study indicated that the energy of the seismic noise recorded by the array is related to the wave height on the ocean and that the H/V ratio for the different sensors is stable in time.

In order to better investigate and understand the wave propagation in the Evergreen Basin, we perform a systematic analysis of the propagation of surface waves in the basin, not only for a single earthquake, but for a set of earthquakes and study the correlation between surface wave types (Love, Rayleigh) and earthquake characteristics (location, magnitude). Therefore, 22 regional earthquakes in distances between 40 and 600 km are selected and the repartition and azimuth angles of Love and Rayleigh waves are investigated in different frequency ranges. Furthermore, by combining the data for the different events, we obtain Love and Rayleigh wave dispersion curves as well as Rayleigh wave ellipticity curves.

THE MUSIQUE ALGORITHM

The first processing step of the MUSIQUE algorithm (Hobiger *et al.*, 2011) is the use of "classical" MUSIC (Schmidt, 1986), an algorithm based on the separation of signal and noise subspaces. Using an array composed of N three-component seismic sensors, the data of all sensors in the frequency domain are given by three (complex) data vectors $\boldsymbol{X}_i(f)$ (each of size $N \times 1$), where $i = 1$ for the vertical, $i = 2$ for the eastern and $i = 3$ for the northern component. For each component, a covariance matrix $\boldsymbol{S}_i(f)$ of size $N \times N$ is calculated by

$$\boldsymbol{S}_i(f) = E(\boldsymbol{X}_i(f)\, \boldsymbol{X}_i^{\dagger}(f)), \tag{1}$$

where $E(x)$ denotes the expectation value and † stands for complex conjugation. In order to include the data of all three sensor components, the three resulting covariance matrices are simply added to form a single covariance matrix $\boldsymbol{S}(f)$ whose associated eigenvectors and eigenvalues are calculated. The eigenvectors associated to the largest eigenvalues span the signal subspace. The remaining eigenvectors span the noise subspace $\boldsymbol{G}$. Azimuth θ and slowness s of the most energetic wave arrivals are identified by maximizing the MUSIC functional

$$P = 1/(\boldsymbol{a}^{\dagger}\, \boldsymbol{G}\, \boldsymbol{G}^{\dagger}\, \boldsymbol{a}), \tag{2}$$

where the steering vector $\boldsymbol{a}$ and the wave vector $\boldsymbol{k}$ are given by

$$\boldsymbol{a} = \exp(-i\, \boldsymbol{R}\, \boldsymbol{k}) / \mathrm{sqrt}(N), \tag{3}$$

$$\boldsymbol{k} = -2\, \pi f\, s(f)\, (\sin\theta, \cos\theta, 0)^{T}, \tag{4}$$

$\boldsymbol{R}$ is the sensor position matrix and the slowness is denoted by $s(f)$. A two-dimensional grid search for the wave azimuth θ and slowness s identifies the values maximizing P.

In order to separate the radial and transverse components of particle motion, the horizontal components are projected in the identified azimuth direction to form the radial signal $\boldsymbol{X}_{radial}(f)$ and the transverse signal $\boldsymbol{X}_{transverse}(f)$. Based on the energy of these signals, Love and Rayleigh waves are distinguished in the following way: If the transverse component carries more energy than the sum of the radial and vertical components, the wave is identified as a Love wave. In the opposite case, it is identified as a possible Rayleigh wave. For Love waves, the processing stops here.

For Rayleigh waves, the polarization between the radial and vertical component is of major interest. In the MUSIQUE algorithm, the estimation of this polarization relationship is performed using the quaternion-MUSIC algorithm (Miron *et al.*, 2005, 2006). This algorithm is based on quaternions, hypercomplex numbers of dimension 4 (*e.g.* Ward, 1997). A thorough presentation of quaternions would be far beyond the scope of this article, but we will briefly introduce the fundamental concept here. Quaternions can be understood as an extension of complex numbers. Instead of using a single complex imaginary unit i, three different imaginary units $\mathtt{i}$, $\mathtt{j}$ and $\mathtt{k}$ are used, satisfying

$$\mathtt{i}^2 = \mathtt{j}^2 = \mathtt{k}^2 = \mathtt{i}\ \mathtt{j}\ \mathtt{k} = -1. \tag{5}$$

The advantage of the quaternion formulation is the following: The analysis of the polarization of Rayleigh waves requires the data of the radial and vertical components. Both are given as complex-valued data vectors $\boldsymbol{X}_{radial}(f)$ and $\boldsymbol{X}_{vertical}(f)$ (both of size $N \times 1$). Using the quaternion formulation, it is possible to merge both data vectors into a single data vector $\boldsymbol{X}_q(f)$ by

$$\boldsymbol{X}_q(f) = \mathtt{Re}(\boldsymbol{X}_{vertical}(f)) + \mathtt{i}\, Re(\boldsymbol{X}_{radial}(f)) + \mathtt{j}\, Im(\boldsymbol{X}_{vertical}(f)) + \mathtt{k}\, Im(\boldsymbol{X}_{radial}(f)). \tag{6}$$

In this way, the polarization relation between both components remains naturally preserved in the data. The quaternion-valued covariance matrix $\boldsymbol{S}_q(f)$ (of size $N \times N$) is then built in the same way as described in equation (1) and the quaternion-MUSIC functional is analog to equation (2), but the quaternion-MUSIC steering vector is given by

$$\boldsymbol{a}_q = [\cos\rho + \mathtt{i} \sin\rho \exp(\mathtt{j}\, \varphi)] \exp(-\mathtt{j}\, \boldsymbol{R}\, \boldsymbol{k}) / \mathrm{sqrt}(N), \tag{7}$$

where φ is the phase difference between the vertical and radial components and ρ the amplitude parameter. The ellipticity is given as $\tan\rho$.

The original quaternion-MUSIC algorithm includes a four-dimensional grid search for the four parameters: azimuth θ, slowness s, phase difference φ and amplitude parameter ρ. Nevertheless, both azimuth and slowness have already been estimated in the first step, and the two remaining parameters can be determined in an analytical way. In theory, retrograde particle motion corresponds to a phase shift of $\varphi = 90°$ between vertical and radial component and prograde motion to $\varphi = 270°$. To allow deviations from these theoretical values, waves with phase differences in the range [45°, 135°] are identified as retrograde waves and waves with phase differences in [225°, 315°] as prograde waves, leaving the intermediate values unclassified.

In this way, the MUSIQUE code estimates azimuth θ and slowness s, identifies Love and Rayleigh waves and evaluates the polarization parameters φ and ρ of Rayleigh waves, distinguishing between retrograde and prograde particle motion.

ARRAY SETUP

In early 1999, the United States Geological Survey (USGS) deployed an array of Kinemetrics K2 accelerometers in the eastern part of the Santa Clara Valley, *i.e.* in the Evergreen Basin. The different instruments were operated in triggered mode. The array layout is shown in Fig. 2 (a) and the array response corresponding to the stations selected for this study in Fig. 2 (b). The P- and S-wave velocities along the profile marked in Fig. 2 (a) are indicated in Fig. 2 (c) and (d), respectively. Along this profile, the thickness of the sedimentary filling of the basin reaches more than 5 km. The velocity profiles were obtained using the USGS San Francisco Bay Area Model of seismic velocities (USGSBayAreaVM-08.3.0), which is based on the works of Brocher *et al.* (2005) and Phelps *et al.* (2008). For this model, the theoretical Rayleigh and Love wave dispersion curves for the structure beneath the different array stations have been calculated.

The south-western stations of the array are located on the border of the Evergreen Basin. Therefore, their dispersion curves are different from those of the central stations. Consequently, for this study we used only the 25 seismic stations in the basin center, which are indicated by the red circles in Fig. 2 (a). As the structure of the basin underneath these stations is rather homogeneous, their respective dispersion and ellipticity curves are very similar. To give an example, the dispersion curves for the station marked by a green circle in Fig. 2 (a) are shown in Fig. 2 (e) and the ellipticity curves in Fig. 2 (f). As the velocity contrast of the model is not very large, the group slownesses of both surface wave types do not show a distinct Airy phase. Furthermore, the theoretical ellipticity curve for the fundamental mode does not exhibit a singularity. Consequently, the motion of this mode should be retrograde at all frequencies. As the motion of the first harmonic mode is prograde, both modes should be separable by the sense of rotation of their particle motion.

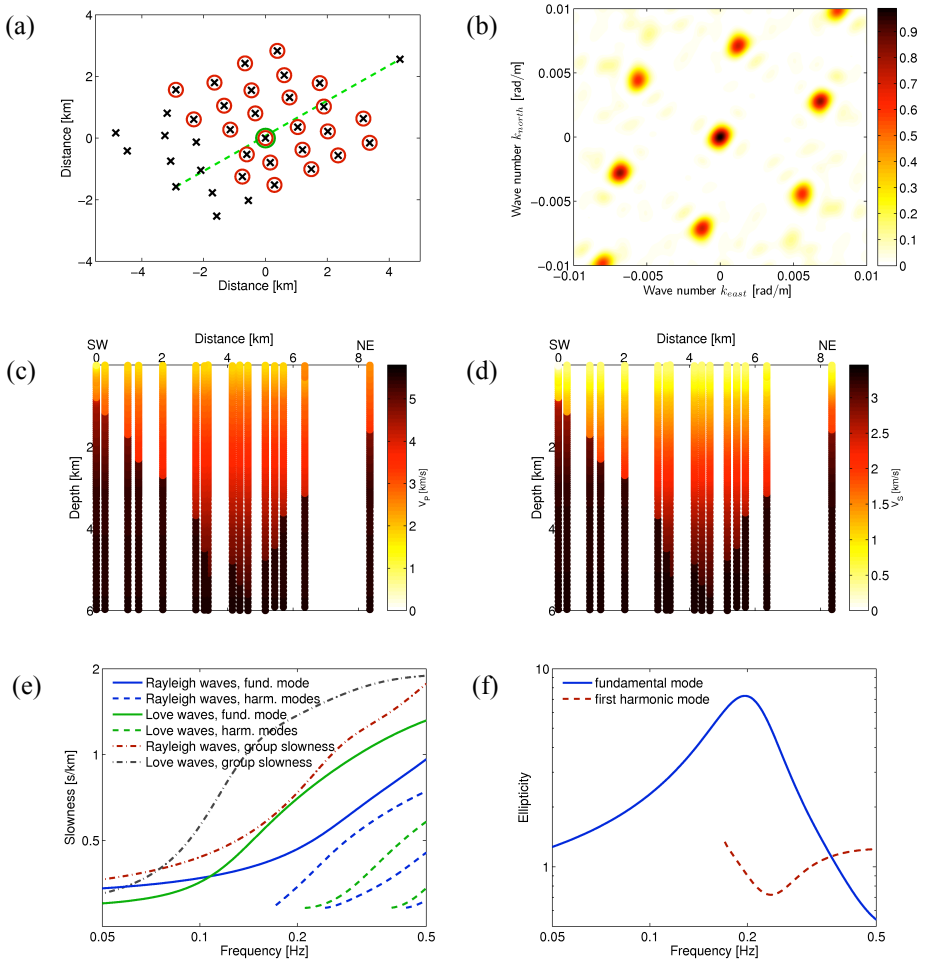

Fig. 2. (a) Layout of the San Jose array. Only the stations marked by a red circle have been used for this study. (b) Theoretical array response for the used array composition. (c) Pressure wave and (d) shear wave velocity profiles according to the basin model along the cross section indicated by the dashed green line in (a). (e) Dispersion curve for phase and group slownesses of Rayleigh and Love waves calculated for the basin model at the central station marked by the green circle in (a). (f) Rayleigh wave ellipticity curve calculated for the basin model at the same station.

DATABASE

The San Jose array recorded a total of 148 earthquakes between May 1999 and May 2004. However, during this time, some stations of the array were subsequently moved to locations at other places in the Santa Clara Valley, reducing the number of recording stations for earthquakes occurring in the late phase of the deployment. As the different seismic sensors were triggered, the total number of stations actually recording a seismic event depends on the magnitude and distance of the earthquake. In order to have a good signal-to-noise ratio and as much seismic sensors as possible for the array analysis, we selected 22 earthquakes whose properties are given in Table 1 for our analysis. Figure 3 shows the epicenters of the respective events.

Table 1. List of analyzed earthquakes. For each earthquake, the origin date and time, location, depth and magnitude are indicated. Furthermore, the distances between the epicenter and the center of the sensor array are given with the theoretical azimuth under which the array should detect the seismic waves. Finally, the number of seismic stations contributing to the analysis of the given earthquake is indicated as well as the recorded signal length for which the indicated number of stations recorded simultaneously.

Event ID	Date	Origin time (UTC)	Latitude [°W]	Longitude [°N]	Depth [km]	Magni-tude	Distance to array [km]	Incident azimuth [°]	Number of Stations	Signal length [s]
1	05/15/1999	13:22	37.53	118.82	5.6	5.6 Mw	269	85	23	436
2	05/15/1999	17:54	37.51	118.83	7.4	4.7 Mw	268	86	23	136
3	08/01/1999	16:06	37.40	117.12	1.3	4.6 Md	420	88	24	540
4	08/18/1999	01:06	37.91	122.69	6.8	5.0 ML	94	310	19	203
5	10/16/1999	09:46	34.59	116.27	0.0	7.1 Mw	590	120	23	1317
6	09/03/2000	08:36	38.38	122.41	10.1	5.2 ML	122	337	21	305
7	09/26/2000	07:20	38.66	119.53	9.2	4.2 ML	250	54	22	104
8	12/02/2000	15:34	39.38	120.45	14.3	4.9 ML	255	28	12	107
9	08/10/2001	20:19	39.81	120.62	4.0	5.5 ML	292	21	18	216
10	12/28/2001	21:14	36.64	121.25	6.8	4.7 ML	98	146	19	191
11	05/14/2002	05:00	36.97	121.60	7.2	4.9 ML	51	153	19	106
12	09/25/2002	07:08	36.59	121.20	8.0	3.9 ML	105	146	13	76
13	11/24/2002	14:54	37.76	121.95	11.0	3.9 ML	44	350	15	98
14	11/25/2002	03:57	37.76	121.94	10.0	3.8 ML	44	350	15	74
15	11/25/2002	18:22	37.76	121.94	11.0	3.5 ML	44	351	12	67
16	11/26/2002	12:38	37.76	121.95	10.6	3.6 ML	44	350	15	72
17	01/07/2003	22:29	36.81	121.39	8.9	4.3 Mw	76	146	15	134
18	02/02/2003	16:22	37.75	121.95	16.8	3.6 ML	42	350	15	70
19	02/02/2003	18:22	37.74	121.94	16.7	4.2 ML	42	350	15	103
20	02/02/2003	18:47	37.75	121.95	16.9	4.0 ML	42	350	15	103
21	02/02/2003	19:02	37.75	121.95	17.1	3.5 ML	43	350	16	56
22	05/25/2003	07:09	38.46	122.70	5.4	4.3ML	141	329	12	145

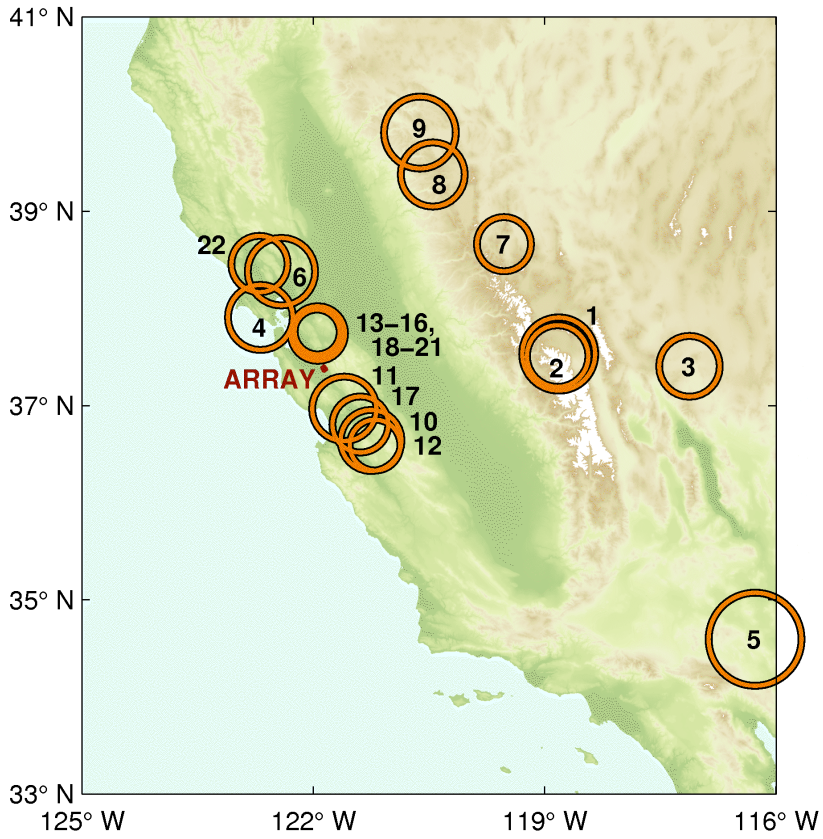

Fig. 3. Map showing the epicenters of the analyzed earthquakes with respect to the location of the San Jose Dense Seismic Array. The diameters of the circles are proportional to the magnitudes of the respective earthquakes.

AZIMUTHAL ENERGY REPARTITION

According to Table 1, there are 4 events in the data set for which the actual recording time is significantly longer than 3 minutes. This allows us to compare the early arrivals of the respective events with the late signal, *i.e.* when no direct waves are present in the data any more and the wave field is mainly composed of scattered waves. We will show the results for event 1, whose epicenter is located to the east of the array. In Fig. 4, the energy distribution with respect to the incident angle for this event is plotted for Rayleigh and Love waves in different frequency ranges. In Fig. 4 (a-f), both Love and Rayleigh wave energies are normalized to their respective maximum. The relative energy distributions of Rayleigh and Love waves which are indicated in Fig. 4 (g-h) are normalized in such a way that the sum of the total energies of Love and Rayleigh waves over all frequency ranges equals 1.

In the early signal (the first 75 s), the main Love wave arrivals are principally coming from the direction of the epicenter, *i.e.* under an azimuth of 85° in all frequency ranges (Fig. 4 (a-c)). The small deviations to the north can be explained by wave refraction at the eastern basin edge. Actually, the north-western to south-eastern orientation of the basin refracts waves arriving from the east by some degrees to the south, so that the array detects them from a direction shifted to the north.
At low frequencies (below 0.3 Hz), Rayleigh waves arrive principally from the epicenter direction, but their amplitude is very low (Fig. 4 g). At higher frequencies, prograde Rayleigh waves are still arriving from eastern directions, but are more scattered than Love waves, whereas retrograde Rayleigh waves are even arriving from the southwest.

In the late signal (after 200 s, Fig. 4 (d-f)), the total energy content is ten times lower than in the early signal and the Love wave energy is significantly larger than the Rayleigh wave energy (Fig. 4 (h)). At all frequencies, a dominant Love wave contribution arriving from the south can be seen, with minor contributions from other directions. This signal from the south has already been observed by Frankel *et al.* (2001) who attributed it to scattered Love waves. The scatterer could be either a large rock formation located south of the array or the southern basin edge (see Fig. 1).
For Rayleigh waves, the energy distribution is rather inhomogeneous, but the most energetic part of Rayleigh waves, retrograde waves between 0.2 and 0.3 Hz, are also arriving from the south.

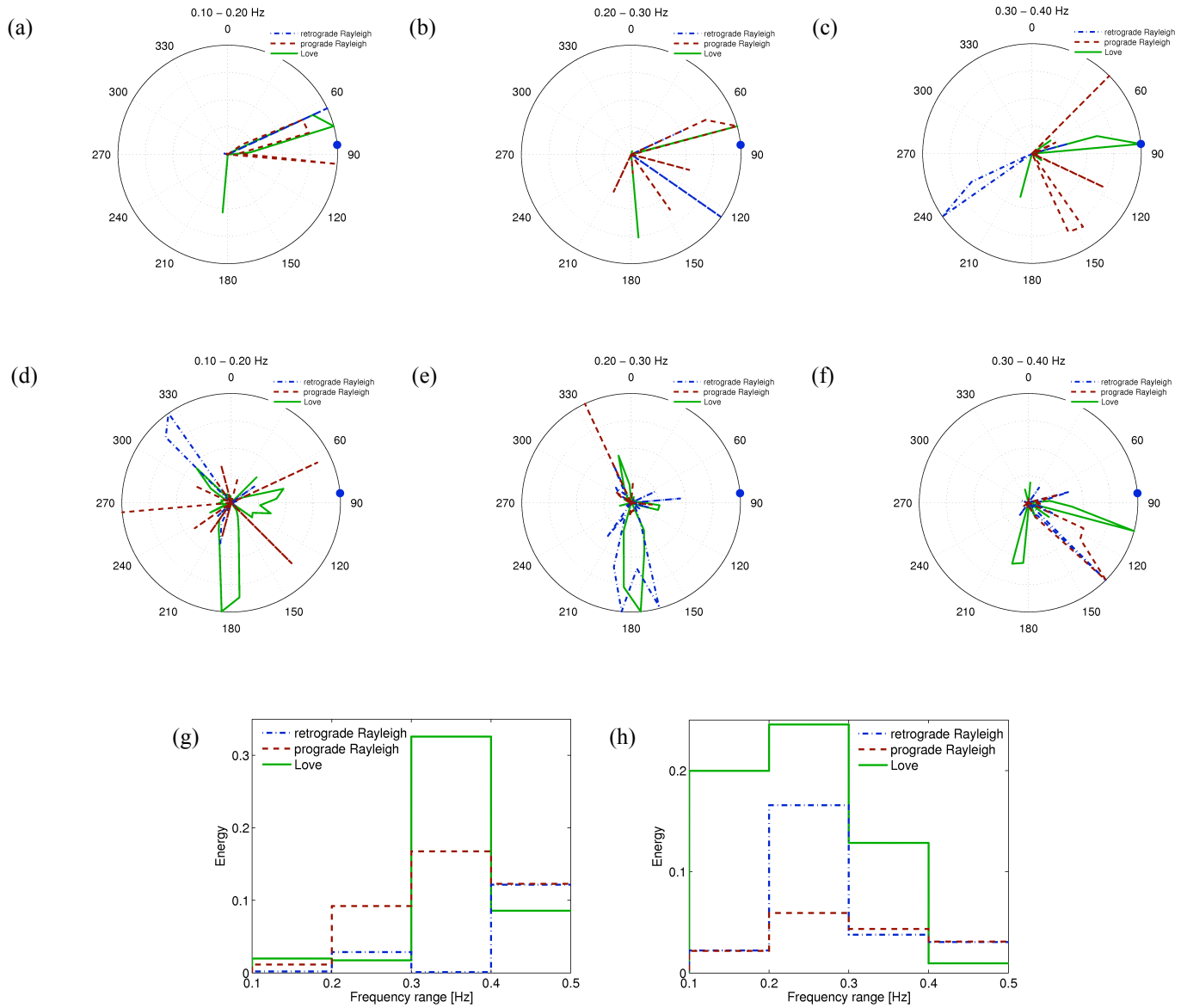

Fig. 4. Azimuthal energy distribution for different frequency ranges for (a-c) the first 75 s of signal and (d-f) the signal after 200 s for the recordings of event 1. The blue dot indicates the epicenter direction. The curves for all different wave types are normalized to their respective maxima. (g) and (h) give the relative energy distribution in the respective frequency ranges for the early and the late signal, normalizing the total energy in the early and late signal to 1, respectively.

For the other events, the detailed pattern of scattered waves is evidently different. However, by combining the analysis results for all 22 events and neglecting all waves arriving within 45° of the respective epicenter direction, we can analyze the scatterers in the basin structure. The results are shown in Fig. 5. Scattered Love waves arriving from the south can be observed at all frequencies. At frequencies below 0.3 Hz, scattered Rayleigh waves are also generated at the southern basin border, while energetic retrograde Rayleigh waves are arriving from the eastern basin border for frequencies above 0.3 Hz. However, most of the prograde Rayleigh wave energy is arriving from the south between 0.4 and 0.5 Hz.

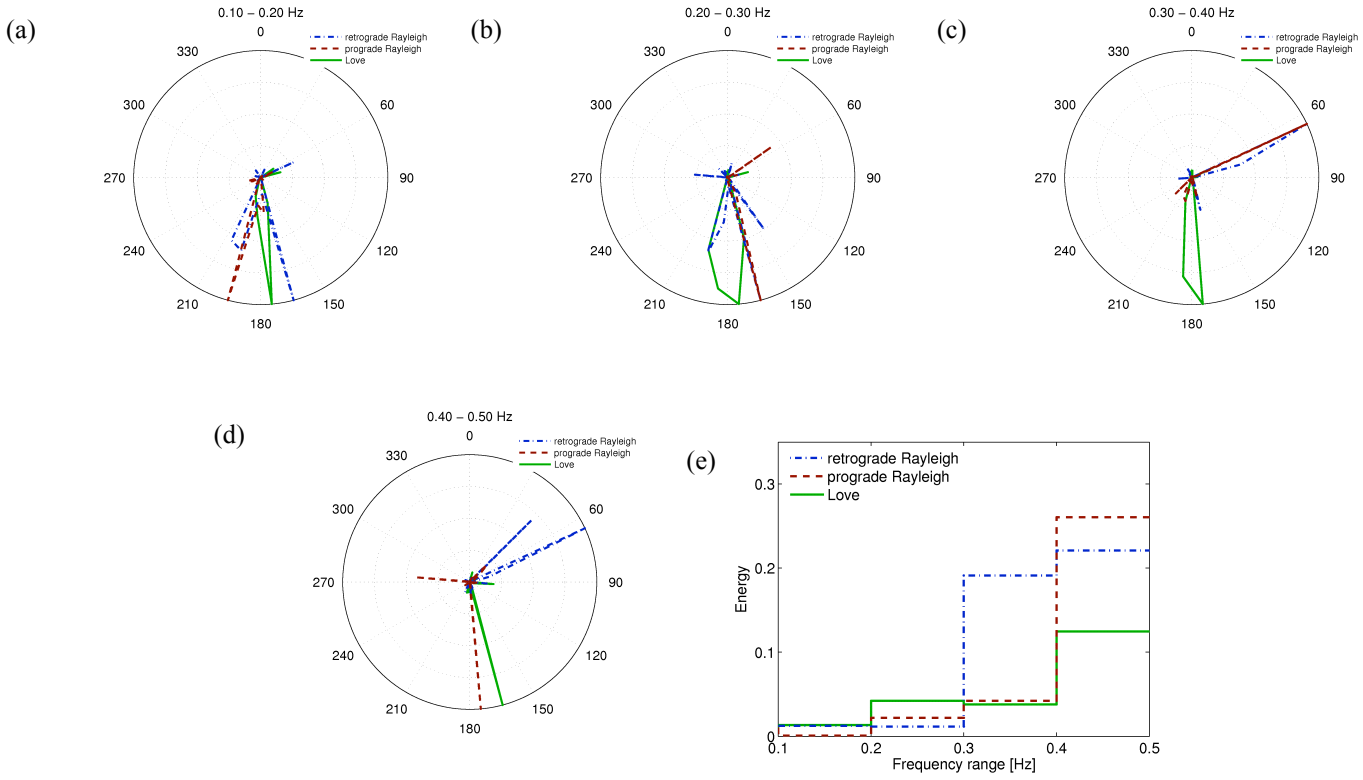

Fig. 5. (a-d) Scattered energy for different frequency ranges, combining all 22 events. The figures have been obtained by omitting all wave arrivals within 45° from the direct azimuth for the respective events. (e) gives the relative energy distribution in the respective frequency ranges.

DISPERSION CURVES

The energy repartition between Love and Rayleigh waves is varying from one earthquake to another. Consequently, the different events reveal different parts of the dispersion curves. We cannot show the dispersion curves for all events here, but limit us to some relevant examples.
The most energetic event, the Hector Mine earthquake (event 5), generated a large proportion of Love waves. The Love wave dispersion curve for this event is compared to the theoretical dispersion curves for the basin model in Fig. 6 (a). The Love wave dispersion curve of the fundamental mode is relatively well retrieved, but no evidence for the presence of higher modes is visible. The two series of events 13-16 and 18-21 have been combined because their epicenters lie very close (see Table 1 and Fig. 3). They show a dispersion curve which is actually very close to the theoretical dispersion curve for the first harmonic mode of Love waves (Fig. 6 (b)). In the data for other events, the first higher Love wave mode is not visible.

The slowness values which were calculated for all events separately are combined to a single Love wave dispersion curve in Fig. 6 (c). This curve has been obtained by summing the data for the single events after normalizing them by their respective total energies. In this way, the information of the most energetic events does not mask the information of less energetic events. The dispersion curve of the fundamental Love wave mode is found between 0.15 and 0.5 Hz, the first harmonic mode is clearly visible between 0.3 and 0.5 Hz.

Compared to the Bay Area Model, our dispersion curve measurements for both Love wave modes are in good agreement in their respective higher frequency parts, but shifted to lower slowness values in their low frequency parts. This confirms the superficial structure of the Bay Area Model, but indicates that the velocities of the deeper layers might be underestimated in this model.

For retrograde Rayleigh waves, some data points can be seen between 0.2 and 0.5 Hz in Fig. 6 (d). As their values are very close to the measured Love wave dispersion curve, it is not clear whether these are well-identified Rayleigh waves or misidentified Love waves. For the prograde Rayleigh waves in Fig. 6 (e), clear data can only be seen above 0.2 Hz. The large spot identified at 0.4 Hz could represent the first harmonic Rayleigh wave mode and is clearly separated from the first harmonic Love wave mode. Nevertheless, from the analysis of retrograde and prograde Rayleigh waves, it is difficult to retrieve a clear dispersion curve. This is certainly due to the fact that the wave field is dominated by Love waves, which bias the estimation of Rayleigh wave dispersion curves.

An alternative way of analyzing the data without taking Love waves into account is to use the vertical component of the signals only. However, the polarization characteristics of the waves, *i.e.* retrograde or prograde sense of motion as well as ellipticity, cannot be retrieved in this case. The resulting dispersion curve for this analysis is shown in Fig. 6 (f). The data form a large cloud of points which covers the theoretical dispersion curves for the basin model's fundamental and first harmonic Rayleigh wave modes. It cannot be determined to which mode the data points correspond or if they correspond to a mixture of both modes. However, the cloud of points is clearly distinguished from the Love wave dispersion curve of Fig. 6 (c). This suggests that the retrograde Rayleigh wave dispersion curve of Fig. 6 (d) is actually biased by Love waves. Nevertheless, the prograde Rayleigh wave of Fig. 6 (e) is not retrieved in Fig. 6 (f) either as it might be masked by the large cloud of points.

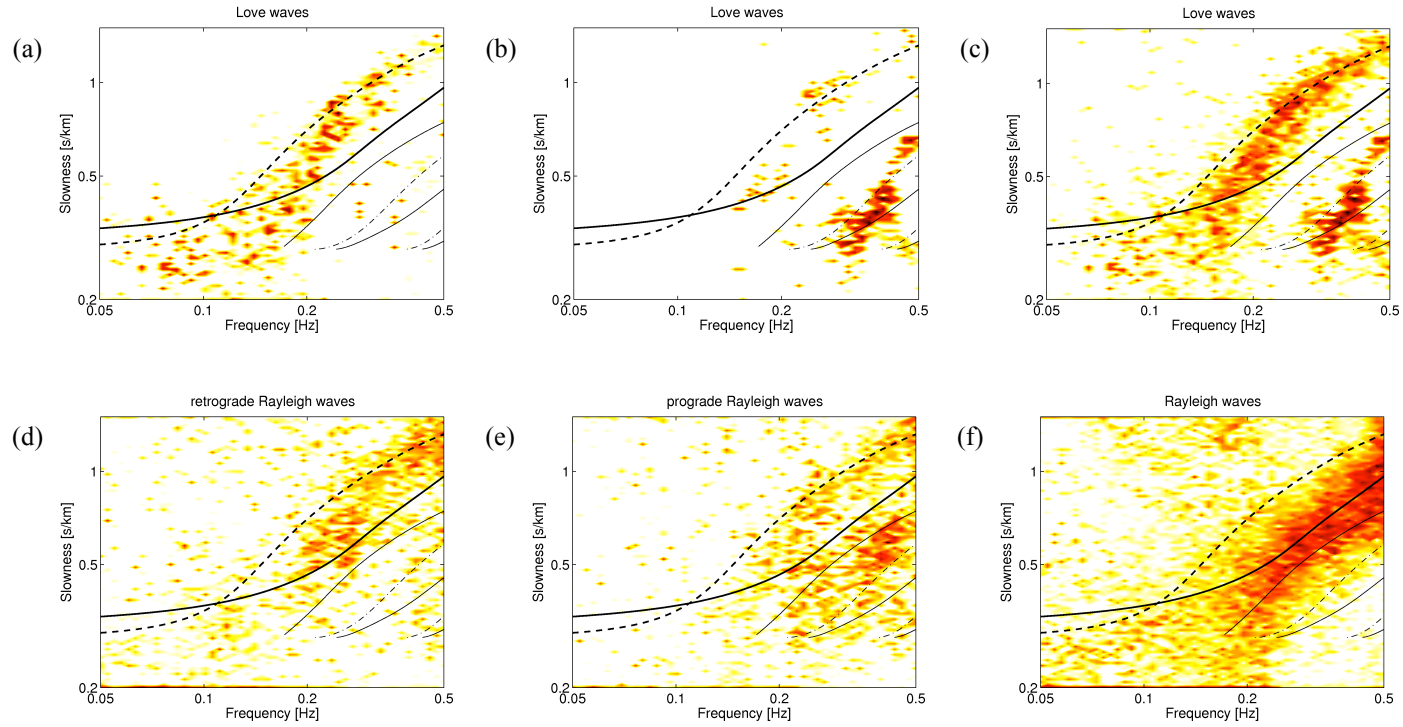

Fig. 6. (a-c) Measured Love wave slowness values for (a) event 5, (b) the combination of events 13-16 and 18-21 and (c) the combination of all events.(d-f) Measured Rayleigh wave slowness values for the combination of all events for (d) retrograde and (e) prograde Rayleigh waves. (f) has been obtained by analyzing the vertical component only, thus suppressing Love waves, but neglecting the difference between retrograde and prograde waves. The slowness values for all measured time windows attributed to the respective wave type are included in the figure, weighted by their respective total energy. The darkest colors indicate high data concentrations. The solid black lines represent the fundamental and harmonic Rayleigh wave dispersion curves corresponding to the basin model for the central station, the dashed and dash-dotted lines the fundamental and harmonic Love wave dispersion curves.

ELLIPTICITY CURVES

The ellipticity curves estimated by MUSIQUE combining the results of all events are shown in Fig. 7 for retrograde and prograde Rayleigh waves. The retrograde ellipticity curve is badly estimated and no ellipticity curve can be identified. For the prograde Rayleigh waves, a scattered ellipticity curve is retrieved, which can be attributed to the first harmonic mode. Below about 0.18 Hz, very few prograde waves are identified compared to the higher frequency part. According to the basin model, the first harmonic mode does not exist below 0.17 Hz. Actually, the estimated ellipticity values are close to the first harmonic mode of the Bay Area Model. This is further evidence that the fundamental mode does not exhibit a singularity. If such a singularity existed, the motion of the fundamental mode of Rayleigh waves would be prograde for the frequency range of the right flank of the peak and consequently bias the ellipticity estimation of the first harmonic mode.

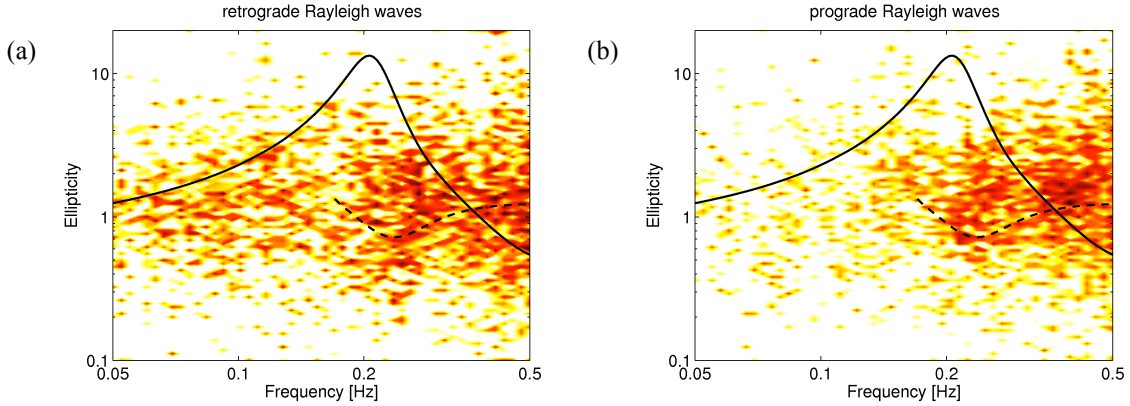

Fig. 7. Measured ellipticity values for (a) retrograde Rayleigh waves and (b) prograde Rayleigh waves, combining the results for all events. The ellipticity values for all measured time windows attributed to the respective wave type are included in the figure, weighted by their respective amplitude. The darkest colors indicate high data concentrations. The solid and dashed black lines represent the ellipticity curves of the fundamental and the first harmonic mode of Rayleigh waves, respectively, calculated using the basin model at the central array station.

CONCLUSION

This study investigated the seismological wave field which was generated by regional earthquakes in the Evergreen Basin, California, using MUSIQUE. In addition to the determination of wave azimuth and velocity, this technique allows the identification of Love, retrograde and prograde Rayleigh waves. For all seismic events, a large amount of the Love wave energy arrives from the south, even for northern earthquakes. Frankel *et al.* (2001) already found evidence for a Love wave scatterer located south of the array and attributed it either to a rock formation or to the southern basin edge. Apart from these scattered Love waves, direct Love waves arrive under azimuths which are slightly deviated from the theoretical earthquake azimuths. The deviations are likely to be explained by refraction of incident waves at the lateral borders of the basin.
Rayleigh waves are more scattered and arrive under a multitude of different azimuths. As a detailed model of the San Francisco Bay Area exists, numerical simulations could help to better understand the propagation patterns and identify the most important wave scatterers. This might also help to understand the relations between earthquake characteristics, surface wave mode generation (fundamental and harmonic modes) and the propagation of surface waves.

For the events located the closest to the array (about 40 km), the first harmonic Love wave mode dominates the wave field. For the other events, no harmonic Love waves of significant amplitude can be identified. They might be produced during those earthquakes as well, but attenuated on their way to the array or this might be a feature attributed to the special location of the close earthquakes. By combining the information of all earthquakes, we succeeded in retrieving the Love wave dispersion curves for the fundamental and the first higher mode. The measured dispersion curves are in good agreement with the Bay Area Model at the higher frequency parts of the respective modes, but faster than the model curves at the low frequency parts. This indicates that the model might underestimate the actual wave velocities of the deeper layers.
The dispersion curve found for retrograde Rayleigh waves is very close to the measured Love wave dispersion curve and could be biased by Love waves as well, particularly because the curve is completely different from the curve obtained by analyzing the vertical components of the signal only. Furthermore, no ellipticity curve can be attributed to these waves. For prograde Rayleigh waves, however, it is possible to identify the dispersion curve and assign an ellipticity curve.

The inter-sensor spacing of the array sets the upper frequency limit of our analysis. Furthermore, the structure of the basin is not absolutely homogeneous underneath the entire used array. Therefore, a smaller, but denser array located in the central part of the basin would allow us to study the higher-frequency part of incident waves. This might help to further increase the understanding of the surface wave propagation in the Santa Clara Valley.

ACKNOWLEDGMENTS

We would like to thank Arthur Frankel and David Carver for kindly providing the data and Arthur Rodgers for supplying the data of the San Francisco Bay Area model and for fruitful discussions.

REFERENCES

T. M. Brocher, E. E. Brabb, R. D. Catchings, G. S. Fuis, T. E. Fumal, R. C. Jachens, A. S. Jayko, R. E. Kayen, R. J. McLaughlin, T. Parsons, M. J. Rymer, R. G. Stanley, and C. M. Wentworth [1997]. "A crustal-scale 3-D seismic velocity model for the San Francisco Bay area, California". Eos Trans. AGU, 78:F435.

D. Dolenc and D. Dreger [2005a]. "Microseisms observations in the Santa Clara Valley, California", Bull. Seismol. Soc. Am., 95:1137–1149, doi: 10.1785/0120040060.

D. Dolenc, D. Dreger, and S. Larsen [2005b]. "Basin structure influences on the propagation of teleseismic waves in the Santa Clara Valley, California", Bull. Seismol. Soc. Am., 95:1120–1136, doi: 10.1785/0120040059.

J. B. Fletcher, J. Boatwright, and A. G. Lindh [2003]. "Wave propagation and site response in the Santa Clara Valley", Bull. Seismol. Soc. Am., 93:480–500.

A. Frankel, D. Carver, E. Cranswick, T. Bice, R. Sell, and S. Hanson [2001]. "Observations of basin ground motions from a dense seismic array in San Jose, California". Bull. Seismol. Soc. Am., 91:1–12, 2001.

S. Hartzell, D. Carver, R. A. Williams, S. Harmsen, and A. Zerva [2003]. "Site response, shallow shear-wave velocity, and wave propagation at the San Jose, California, Dense Seismic Array", Bull. Seismol. Soc. Am., 93:443–464, doi: 10.1785/0120020080.

S. Hartzell, S. Harmsen, R. A.Williams, D. Carver, A. Frankel, G. Choy, P.-C. Liu, R. C. Jachens, T. M. Brocher, and C. M. Wentworth [2006]. "Modeling and validation of a 3D velocity structure for the Santa Clara Valley, California, for seismic-wave simulations", Bull. Seismol. Soc. Am., 96:1851–1881, doi: 10.1785/0120050243.

S. Hartzell, L. Ramirez-Guzman, D. Carver, and P. Liu [2010]. "Short baseline variations in site response and wave-propagation effects and their structural causes: Four examples in and around the Santa Clara Valley, California", Bull. Seismol. Soc. Am., 100:2264–2286, doi: 10.1785/0120090278.

M. Hobiger, C. Cornou, P.-Y. Bard, and N. Le Bihan [2011], "MUSIQUE: A quaternion-based array processing technique for surface wave polarization analysis," IEEE Worshop on Statistical Signal Processing (SSP2011), Nice, France, 28-30 June, 2011.

S. Miron, N. Le Bihan, and J. I. Mars [2005], "High resolution vector-sensor array processing using quaternions", IEEE International Conference on Statistical Signal Processing, Bordeaux, France, 2005.

S. Miron, N. Le Bihan, and J. Mars [2006]. « Quaternion-MUSIC for vector-sensor array processing", IEEE Trans. Signal Process., 54:1218–1229.

G. A. Phelps, R. W. Graymer, R. C. Jachens, D. A. Ponce, R. W. Simpson, and C. M. Wentworth [2008]. "Three-dimensional geologic map of the Hayward Fault zone, San Francisco Bay region, California", U.S. Geological Survey Scientific Investigations Map 3045, http://pubs.usgs.gov/sim/3045/.

R. O. Schmidt [1986]. "Multiple emitter location and signal parameter estimation", IEEE Trans. Antennas and Propagation, 34:276–280.

C. M. Wentworth [1997], "Geologic materials of the San Francisco Bay region", U.S. Geological Survey Open-File Report 97-744, part 5.

J. P. Ward [1997], "Quaternions and Cayley Numbers: Algebra and Applications", Kluwer Academic Publishers, Dordrecht, The Netherlands.